JOURNAL OF SOLID STATE CHEMISTRY **96,** 72–83 (1992)

Crystal Chemistry and Transport Properties of $Nd_{2-x}A_xNiO_4$ (A = Ca, Sr, or Ba, $0 \leq x \leq 1.4$)

Y. TAKEDA,* M. NISHIJIMA, N. IMANISHI, R. KANNO,† AND O. YAMAMOTO

Department of Chemistry, Faculty of Engineering, Mie University, Kamihama-cho 1515, Tsu, Mie-ken 514, Japan

AND M. TAKANO

Institute for Chemical Research, Kyoto University, Uji, Kyoto-fu 611, Japan

Received May 16, 1991

Structural and electrical properties of the system crystallizing in the K_2NiF_4 structure, $Nd_{2-x}A_xNiO_4$ (A = Ca, Sr, or Ba, $0 \leq x \leq 1.4$), were studied. The solid solution limits of alkaline earth were 0.6, 1.4, and 0.6 for Ca, Sr, and Ba, respectively. Oxygen content was controlled by annealing under various oxygen pressures below 150 atm. Powder X-ray diffraction data were analyzed by the Rietveld method to determine the bond lengths. In the case of the Sr-substituted system, tetragonality in the lattice parameters, c/a, shows a maximum at $x = 0.6$, while distortion of a NiO_6 octahedron, Ni–O(2) (//c-axis)/Ni–O(1) (//a-axis), monotonically decreases from 1.13 ($x = 0$) to 1.04 ($x = 1.4$). No Jahn–Teller distortion appears in a Ni^{3+} region. A metal–semiconductor transition is observed for $0 < x < 1.0$, the transition temperature decreasing from 450 K ($x = 0.1$) to 100 K ($x = 1.0$), but it exhibits a change in character at $x = 0.6$ where the sign of the Seebeck coefficient also changes.

Introduction

Even before the epoch-making discovery of superconductivity in the $La_{2-x}Ba_xCuO_4$ system (*1*), oxides crystallizing in the K_2NiF_4 structure were widely studied for a rich variety of their structural and physical properties (*2*). Among them, special attention has been paid to rare earth nickelates, Ln_2NiO_4 (especially for Ln = La), which undergo a gradual semiconductor–metal transition without any apparent change in structure (*3–5*). The structural and electrical properties are sensitive to the excess oxygen. Recently two types of ordering modes leading to serial oxygen contents hae been found for oxygen rich La_2NiO_{4+n} ($n = \frac{1}{2}n : n > 2$) (*6*). Substitution of Sr for La causes a decrease in resistivity and metal–semiconductor transition temperature (*7, 8*). It is interesting to reveal similarities and dissimilarities of this type of oxide containing Ni and Cu starting from $LnANiO_4$ (A : alkaline earth metal) and La_2CuO_4. Apparently, both crystallize in the same type of structure. Each Ni^{3+} (low spin state) and Cu^{2+}, both $s = \frac{1}{2}$, facilitates

* To whom correspondence should be addressed.

† Present address: Department of Chemistry, Faculty of Science, Kobe University, Nada-ku, Kobe, 657 Japan.

0022-4596/92 $3.00

$2D$ metal–oxygen conductive network formation by lowering its partially filled $3d\gamma$ levels to proximity of the oxygen $2p$ levels by the effects of the high valence (Ni^{3+}) and large atomic numbers. Though $S = \frac{1}{2}$ for both Ni^{3+} and Cu^{2+}, the correlation effects would be much stronger for Cu^{2+} provided with three-quarters-filled $3d\gamma$ levels than for Ni^{3+} characterized by only a quarter-filled level; this would be the most important difference. Anyway, an understanding of these nickelate systems should help in the understanding of the copper superconductors.

Recently we reported detailed structural, transport, and magnetic data for the system $La_{2-x}Sr_xNiO_4$ ($0 \leq x \leq 1.6$) (*8*). A Reitveld analysis of powder X-ray diffraction (XRD) data showed that a maximum of the tetragonality in the lattice parameters, c/a, appeared at $x = 0.6$, while distortion of a NiO_6 octahedron, Ni–O(2) (//c-axis)/Ni–O(1) (//a-axis), monotonically decreased from 1.17 ($x = 0$) to 1.03 ($x = 1.4$). No Jahn–Teller distortion appears in a Ni^{3+} region. A metal–semiconductor transition was observed for $0 \leq x \leq 1.2$, the transition temperature decreasing from 690 K ($x = 0$) to 20 K ($x = 1.2$). For $x > 1.3$, the specimen showed metallic behavior down to 10 K.

Neodymium is the smallest rare-earth metal forming a K_2NiF_4 type lanthanide nickelate. The smaller rare-earth metals than Nd form neither La_2NiO_4 type nor Nd_2CuO_4 type compounds. This is a large difference seen between the rare-earth nickelate and rare-earth cuprate. As Nd_2NiO_{4+z} shows fairly different characters from La_2NiO_{4+z} in structural, electrical, and magnetic properties (*9*), it is interesting to investigate the structural and physical properties of the $Nd_{2-x}A_xNiO_4$ system. Although a considerable number of studies have been reported on the structure, transport and magnetic properties of the $La_{2-x}A_xNiO_4$ system, only a few have been reported for the $Nd_{2-x}A_xNiO_4$ system. Recently, Arbuckle *et al.* reported the electrical and magnetic properties of $Nd_{2-x}Sr_xNiO_4$ ($0 \leq x \leq 1$) (*10*). Unfortunately they have not analyzed the crystal structure, so they concluded that the distortion of local coordination of NiO_6 octahedra follows the changes in the lattice constants. However, as shown in the case of the $La_{2-x}Sr_xNiO_4$ system, there is no relation between the distortion of the NiO_6 octahedron and the tetragonality in the lattice parameters, c/a (*8*). The possibility of transition for the low spin Ni^{3+} configuration from $t_{2g}^6 d_{z^2}^1$ to $t_{2g}^6 d_{x^2-y^2}^1$, as pointed out by many authors (for example, Ref. (*7*)), was excluded.

In this study, we prepared $Nd_{2-x}A_xNiO_4$ ($0 \leq x \leq 1.4$), where A = Ba, Sr, or Ca, and refined the crystal structure by X-ray Reitveld analysis from high temperature (600 K) to low temperature (77 K). Electrical conductivity and the Seebeck coefficient were measured over a wide range of temperature. In this paper some results of our structural and electrical characterizations of $Nd_{2-x}A_xNiO_4$ system are summarized and the transport properties are also discussed.

Experimental

Mixtures of Nd_2O_3, alkaline earth carbonates ($CaCO_3$, $SrCO_3$, or $BaCO_3$), and Ni powder were dissolved in nitric acid. Before use, Nd_2O_3 was dried at 1000°C for 1 hr. The solutions containing each ion in various ratios were dried until the nitrates completely decomposed. The solids formed were calcined at 600°C for 12 hr and heated at 1200°C for 24 hr in 1 atm of O_2 gas flow. To attain oxygen stoichiometry, samples sintered as above were annealed at 500–700°C in vacuum sealed Pyrex tubes with Ti metals as oxygen getters for the composition $x \leq 0.2$ and also annealed under 150 atm of oxygen pressure at 600°C for the higher alkaline earth metal content $x \geq 1.2$.

XRD patterns of powdered samples were obtained on Rigaku RAD-RC (12kw) using monochromated Cu$K\alpha$ radiation and a scintillation detector. For a Reitveld analysis

intensity data were collected at each 0.02° step width for 2 or 3 sec over a 2θ range from 10° to 100°. For some samples, temperature was varied from 77 to 700 K. A computer program (RIETAN) was used for a profile refinement calculation (*11*). The oxidation state of nickel was determined by iodometry. Electrical resistivity was measured by the four probe method using sintered pellets in a temperature range between 15 and 1000 K. The Seebeck coefficient was measured in the temperature range between 77 and 1000 K using home made equipment. The temperature difference was kept in the range of 3–20 K.

Result and Discussion

1. Solid Solution Range of $Nd_{2-x}A_xNiO_4$ (A = Ca, Sr, or Ba)

The synthesis of solid solution $Nd_{2-x}A_xNiO_4$ (A = Ca, Sr, Ba) was tried in the range $0 \leq x \leq 1.8$ by decomposition from the starting nitrates. The solid solution limits of alkaline earth were $x = 0.6$, 1.4, and 0.6 for Ca, Sr, and Ba, respectively. Use of La_2O_3, ACO_3, and NiO yielded smaller ranges of monophasic samples. Listed in Table I are lattice parameters, space groups, and oxygen content of the samples in the single phase region in $Nd_{2-x}A_xNiO_4$. In the case of Ca substitution, CaO and NiO always remained as second phases over $x = 0.6$ though various heating periods, temperatures, and atmospheres were tried for the synthesis. In Sr substitution, monophasic samples until $x = 1.4$ were easily obtained, while the sintered materials of $x > 1.4$ rapidly absorbed the moisture and CO_2 to collapse and decompose to the carbonate and hydroxide. The substitution range of Ba was unexpectedly narrow; the heating of samples for $x > 0.6$ at more than 1200°C yielded partial melting which may be due to the formation of $BaNiO_{3-z}$, and heating at less than 1200°C brought the presence of multiple phases. The stability of the compounds having K_2NiF_4 structure is sometimes discussed with the tolerance factor

$$t = (r_A + r_O)/\sqrt{2}(r_{Ni} + r_O),$$

where $r_A + r_O$ is the optimum cation–oxygen bond length in the rocksalt phases and $r_{Ni} + r_O$ is that in the NiO_2 planes, which are commonly taken as the sums of the ionic radii. Based on Shannon's ionic radii (*12*), the theoretical tolerance factors of alkaline earth substitution limits for $Nd_{2-x}A_xNiO_4$ are $t = 0.87$, 0.98, and 0.90 for Ca ($x = 0.6$), Sr ($x = 1.4$), and Ba ($x = 0.6$), respectively. Judging from the tolerance factor, more substitution of Ca and Ba should be possible. It is necessary to try the synthesis using more reactive starting materials.

These systems allow a wide range of oxygen nonstoichiometry in both oxygen excess ($z > 0$) and oxygen deficit ($z < 0$) directions depending on the synthetic conditions. For the samples $0.3 \leq x \leq 1.0$, the near oxygen stoichiometry was attained by annealing in air or under oxygen gas flow, while annealing under 150 atm of oxygen was carried out at 600°C for 48 hr for $x > 1.2$ (Sr). Below $x = 0.2$, the samples always contained excess of oxygen when prepared under oxidation conditions (for example, $Nd_2NiO_{4.20}$ was obtained under 1 atm of oxygen). On the other hand, the starting mixture never reacted under reductive conditions such as N_2 or Ar gas flows. To reach oxygen stoichiometric composition, the oxygen rich sample sintered as above was annealed in a vacuum sealed Pyrex or silica tube with Ti metal powder as oxygen getter at 500–700°C. However, only the minimum value of $z = 0.11$ for Nd_2NiO_{4+z} was achieved by this method. When the annealing temperature was increased, the decomposition reaction such as $Nd_2NiO_{4+z} \rightarrow x/2Nd_2O_3 + Nd_{2-x}NiO_{4+z'}$ occurred. A stronger reduction at lower temperature will be needed to obtain the stoichiometric Nd_2NiO_4. It is in contrast to the case of La_2NiO_4 that the oxygen stoichiometric

TABLE I

LATTICE PARAMETERS, SPACE GROUPS, AND OXYGEN CONTENT IN THE SYSTEM $Nd_{2-x}A_xNiO_4$

x	a(Å)	b(Å)	c(Å)	Space group	Oxygen content
			A = Ca		
0.0	5.6417(3)	5.4283(2)	12.2106(4)	*Bmab*	4.12
0.1	5.4283(3)	5.3931(2)	12.2235(4)	*Bmab*	4.10
0.2	5.4092(2)	5.3899(2)	12.2384(2)	*Bmab*	4.09
0.3	5.3996(8)	5.3561(8)	12.245(1)	*Bmab*	3.99
0.4	5.3983(1)	5.3202(1)	12.2510(1)	*Fmmm*	4.02
0.5	5.3648(1)	5.3071(1)	12.2724(1)	*Fmmm*	4.05
0.6	5.3539(1)	5.3042(1)	12.2724(2)	*Fmmm*	3.97
			A = Sr		
0.1	5.4415(3)	5.4250(3)	12.2552(4)	*Bmab*	4.10
0.2	3.8191(1)		12.3316(4)	*I4/mmm*	4.04
0.3	3.8023(1)		12.3822(3)	*I4/mmm*	4.06
0.4	3.7827(1)		12.4448(1)	*I4/mmm*	3.95
0.5	3.7752(1)		12.4707(2)	*I4/mmm*	4.05
0.6	3.7723(1)		12.4586(2)	*I4/mmm*	4.02
0.7	3.7750(1)		12.4345(3)	*I4/mmm*	4.02
0.8	3.7877(1)		12.3356(2)	*I4/mmm*	4.06
0.9	3.7972(1)		12.3045(3)	*I4/mmm*	4.04
1.0	3.7968(1)		12.2744(2)	*I4/mmm*	4.03
1.2	3.8020(1)		12.2472(2)	*I4/mmm*	4.04
1.4	3.8993(1)		12.2453(1)	*I4/mmm*	4.05
			A = Ba		
0.1	3.8418(2)		12.3227(8)	*I4/mmm*	4.10
0.2	3.8208(1)		12.4436(2)	*I4/mmm*	4.08
0.3	3.8165(1)		12.5141(3)	*I4/mmm*	4.06
0.4	3.8118(1)		12.5746(1)	*I4/mmm*	4.02
0.5	3.8109(1)		12.6353(2)	*I4/mmm*	4.00
0.6	3.8107(1)		12.6459(2)	*I4/mmm*	3.97

sample was easily prepared under mild reductive conditions. The difference may be due to the ionic size difference between La and Nd (*13*). Smaller Nd ions will enhance the bond length mismatch between the rocksalt and NiO_2 planes; therefore, the excess oxygen is more easily introduced within the rocksalt layer to adjust the mismatch.

The oxygen content for each sample in Table I is the nearest oxygen stoichiometric sample obtained. The space group was determined from the extinction role and pattern profile of XRD. *Fmmm* and *Bmab* were distinguished by the existence of small peaks from $h + k = 2n$ and $h = 1 = 2n$. The tetragonal lattice parameters a and c obtained by Reitveld analysis for these systems are plotted in Fig. 1 against alkaline earth metal content. For a convenient comparison, orthorhombic a_o and b_o parameters were calculated as tetragonal a_t parameter according to the expression $a_t = (a_o + b_o)/2\sqrt{2}$. The c-axis increases with ionic size of doped alkaline metal but the a-axes of Sr and Ca doped metals is almost equal. With increasing x, the a and c parameters for each system show a minimum and a maximum at around $x \cong 0.6$; therefore, the tetragonality

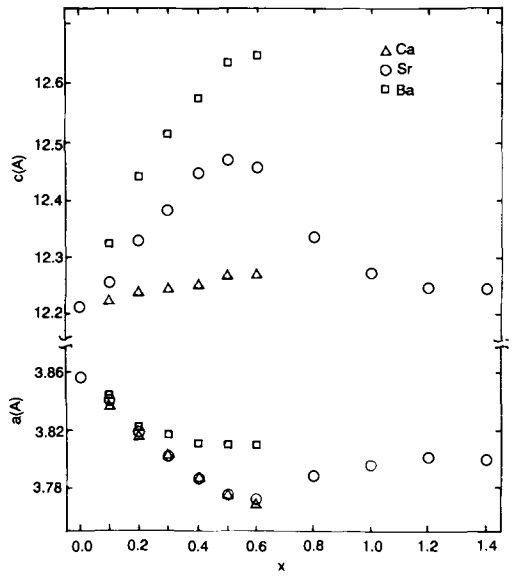

FIG. 1. Variation of the lattice parameters in the $Nd_{2-x}A_xNiO_4$ system. (△) A = Ca, (○) A = Sr, (□) A = Ba.

ratio c/a shows a maximum at the composition $x \cong 0.6$. In the case of Sr, the tetragonality ratio c/a again decreases for $0.6 < x < 1.0$ and becomes constant in $x > 1.0$. This behavior is almost similar to the cases of $La_{2-x}Sr_xNiO_4$ (*8*) and $La_{2-x}Ba_xNiO_4$ (*14*). Our data for the Sr system are slightly different from those of Arbuckle *et al.* (*10*). This may be due to the difference of oxygen content of the samples.

Many authors have explained the increase of the c-axis in the range $x \leq 0.6$ as being due to the Jahn–Teller effect of Ni^{3+} in a low spin state ($d\varepsilon^6 d\gamma^1$) and the decrease for $x > 0.6$ as the transition of $d_{z^2} \rightarrow d_{x^2-y^2}$. K_2NiF_4 structure is built up of alternately stacked single perovskite and double rock-salt layers (Fig. 2). In the scheme of space group *I4/mmm*, for example, Ni and O(1) ions are fixed at special positions, while Nd (or A) and O(2) ions have free parameters, z, along the c axis. Therefore it is not readily apparent that the direction of NiO_6 follows the changes in the lattice constants. In our Reitveld analysis for $La_{2-x}Sr_xNiO_4$, the distortion of the NiO_6 octahedron was revealed to decrease monotonically with increasing x (*8*).

2. *Oxygen Nonstoichiometry in* Nd_2NiO_{4+z}

The sample prepared at 1200°C in air had oxygen content of $z = 0.18$; it was again annealed under various conditions to obtain different oxygen contents. The range we could prepare was from $z = 0.25$ (600°C, Po_2 = 600 atm, 48 hr) to $z = 0.11$ (675°C, with Ti getter in sealed silica tube, 24 hr). Under more reductive conditions, the decomposition reaction, $Nd_2NiO_{4+z} \rightarrow x/2Nd_2O_3 + Nd_{2-x}NiO_{4+z'}$, occurred. In Fig. 3 is shown the variation of the lattice parameters with oxygen content. The abrupt change in parameters is shown at

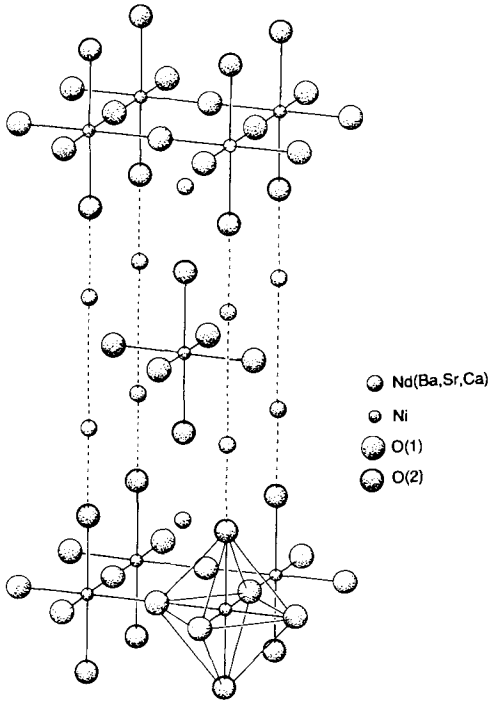

FIG. 2. K_2NiF_4 type structure for $Nd_{2-x}A_xNiO_4$.

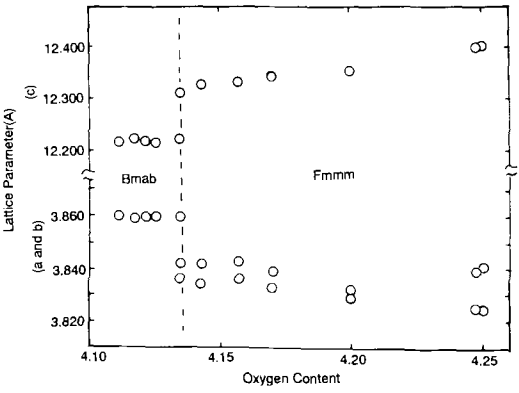

FIG. 3. Variation of the lattice parameters in the Nd_2NiO_{4+z} system.

around $z \cong 0.13$, the oxygen rich region is assumed to belong to the space group *Fmmm* and poor region Bamb on the analogous of La_2NiO_{4+z} by Jorgensen *et al.* (*15*). The XRD pattern below $z < 0.13$ apparently looks like tetragonal *I4/mmm* but the small peaks arising from the lower Bmab symmetry are observed. In the *Fmmm* region the orthorhombic strain is much larger and is easily visible in the raw data. These make a large contrast to La_2NiO_{4+z}, that is, the XRD patterns for oxygen rich La_2NiO_{4+z} appeared to be indexed in the tetragonal *I4/mmm* cell, while those of oxygen stoichiometric La_2NiO_4 can be easily distinguished as orthorhombic. In the *Fmmm* region, *a* and *b* parameters decrease and the *c* parameter increases with increasing oxygen content but in *Bmab* all parameters are constant with oxygen content.

3. Structure of $Nd_{2-x}A_xNiO_4$ (A = Ca, Sr, or Ba) Systems

Structure of $Nd_{2-x}Sr_xNiO_4$ was refined by assuming space group *I4/mmm* for $0.2 \leq x \leq 1.4$. The Nd, Sr, and O(2) ions are located at 4*e* sites with coordinates (0,0,*z*) (*16*). Nd and Sr were assumed to be randomly sited at 4*e* sites. Nonstoichiometric effects on this analysis were examined by changing the occupation factors and/or assuming interstitial O(3) site, but the analytical results were found to be little influenced. The structure for the samples belonging to the space group *Fmmm* was refined as the analogue to $La_2NiO_{4.18}$ (*15*). The Nd(Ca) and O(2) ions are located at (0,0,*z*) with $z = 0.36$ and 0.16, respectively, the Ni ions at (0,0,0), and O(1) at $(\frac{1}{4},\frac{1}{4},0)$. On the other hand, the refinement for the samples of *Bmab* space group were first tried as the analogue to *Bmab* La_2NiO_4 (*15*), but the oxygen parameters to be refined are so numerous that the results were dispersive. So the atomic posi-

TABLE II

POSITIONAL AND THERMAL PARAMETERS FOR TYPICAL COMPOSITIONS OF $Nd_{2-x}Sr_xNiO_4$

Atom	Site		x = 0.2	x = 0.6	x = 1.0	x = 1.4
Nd,Sr	4*e*	z	0.3620(6)	0.3614(5)	0.3613(5)	0.3559(4)
		$B(A^2)$	0.2(1)	0.3(1)	0.4(2)	0.4(4)
Ni	2*a*	$B(A^2)$	0.4(7)	0.3(3)	0.3(3)	0.3(3)
O(1)	4*c*	$B(A^2)$	1.8(11)	0.5(7)	0.3(6)	0.4(5)
O(2)	4*e*	z	0.178(5)	0.171(3)	0.165(3)	0.161(3)
		$B(Å^2)$	1.8(11)	0.5(7)	0.3(3)	0.4(5)
		R_{wp}	15.18	12.17	13.41	12.42
Residuals		R_p	11.63	9.33	9.65	9.14
(%)		R_E	3.06	3.68	3.61	3.37
		R_I	5.17	5.25	4.78	4.36

TABLE III

INTERATOMIC DISTANCES AND BOND ANGLES FOR TYPICAL COMPOSITIONS OF $Nd_{2-x}Sr_xNiO_4$

	$x = 0.2$	$x = 0.6$	$x = 1.0$	$x = 1.2$
Distance (Å)				
Ni–O(1) *a*-axis	1.9096(1)	1.8862(1)	1.8984(1)	1.9002(1)
Ni–O(2) *c*-axis	2.19(6)	2.13(5)	2.03(4)	1.97(3)
Nd–O(2) *c*-axis	2.27(6)	2.37(5)	2.40(4)	2.44(3)
Nd–O(1)	2.557(5)	2.557(4)	2.550(4)	2.562(3)
Nd–O(2) [110]	2.74(1)	2.698(7)	2.705(5)	2.699(3)
Angle (degree)				
Nd–O(2)–Nd [110]	159(3)	163(2)	166(2)	169(2)

tions were fixed to be the same as those for *Fmmm*. Tables II and III list the final structural parameters and interatomic distances for the typical compositions and Fig. 4 shows the Ni–O and Nd(Sr)–O bond lengths plotted vs x in $Nd_{2-x}Sr_xNiO_4$. The most interesting thing to be noted is that the elongation of the NiO_6 octahedron along the *c*-axis is monotonically decreased with increasing x without exhibiting any anomaly at $x = 0.6$ as expected from the variation of the *c* parameter. The degree of the elongation, Ni–O(2)/Ni–O(1), reaches 1.02 at $x = 1.4$. The wavy variation of the *c* axis results from the competing changes of the Nd(Sr)–O(2) bond length that increases to saturation at $x \cong 0.6$ and the Ni–O(2) distance that decreases monotonically up to $x \cong 1.4$. They clearly do not reflect Jahn–Teller enhancement of the tetragonal distortion of the NiO_6 octahedra with increasing Ni^{3+} concentration as previously suggested (*7, 10*). It is impressive to find that the Sr substitution causes the drastic shift of the O(2) ions almost without modifying the *a* axis length. (A slight minimum is observed at $x \cong 0.5$).

The structures of $Nd_{2-x}Ca_xNiO_4$ and $Nd_{2-x}Ba_xNiO_4$ ($0 \leq x \leq 0.6$) were also refined in the same manner as Nd_2NiO_{4+z} and $Nd_{2-x}Sr_xNiO_4$. The Ni–O and Nd(Ca or Ba)–O bond lengths are plotted in Fig. 5 with those of $Nd_{2-x}Sr_xNiO_4$. In spite of the substitution of different sizes of alkaline earth metal, the distances of Ni–O(1) and Ni–O(2) show no remarkable dependence on alkaline earth metal. The effect of substitution was reflected on the Nd(Ca or Ba)–O(2) distance along the *c* axis.

To see the displacement of the in-

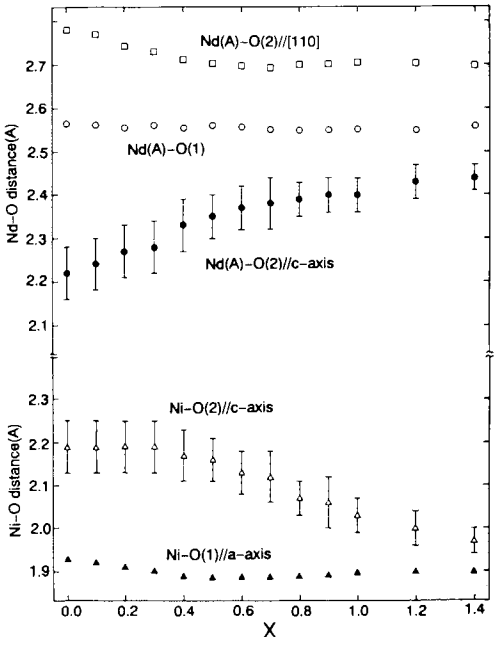

FIG. 4. Variation of Ni–O and Nd(Sr)–O bond distances in the $Nd_{2-x}Sr_xNiO_4$ system. (▲) Ni–O(1)//*a*-axis, (△) Ni–O(2)//*c*-axis, (○) Nd(Sr)–O(1), (●) Nd(Sr)–O(2)//*c*-axis, (□) Nd(Sr)–O(2)//[110].

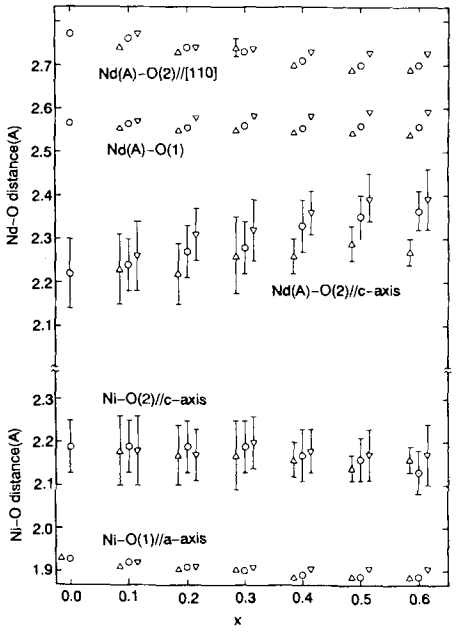

FIG. 5. Variation of Ni–O and Nd(A)–O bond distances in the Nd2$-_xA_xNiO_4$ system. (△) A = Ca, (●) A = Sr, (▽) A = Ba.

teratomic distances on temperature, the high and low temperature XRD was measured for $Nd_{2-x}Sr_xNiO_4$. The cell parameters increase monotonically with temperature, showing no anomaly over the entire temperature interval (Fig. 6). The interatomic distances obtained by Reatveld analysis showed no drastic change with temperature. The variation of Ni–O(1), Ni–O(2), and Nd(Sr)–O(2) distances with temperature are shown in Fig. 7 for $x = 0.3$ and 0.9 as examples.

4. *Transport Properties*

Electrical resistivity data for the system $Nd_{2-x}Sr_xNiO_4$ are given in Fig. 8 and for $Nd_{2-x}Ca_xNiO_4$ and $Nd_{2-x}Ba_xNiO_4$ in Fig. 9. For $x \leq 0.4$ (in the cases of Ca and Ba, $x \leq 0.6$), the resistivity does not depend much on alkaline earth content and is semiconductive with a linear relation between $\log \rho$ and $1/T$. The activation energy for semiconductive region is around 0.1–0.2 eV. For $x \geq 0.6$ in $Nd_{2-x}Sr_xNiO_4$, the resistivity generally decreases as Sr content increases, the minimum value at 300 K of $\rho = 1 \times 10^{-2}\Omega$ cm is attained for $x = 1.2$–1.4. Compositions from $x = 0.6$ to 1.0 display smooth semiconductor–metal transitions with a transition temperature lowering from 450 K ($x = 0.6$) to 100 K ($x = 1.0$) as plotted in Fig. 10. The resistivity in the semiconductive region no longer shows a linear relation between $\log \rho$ and $1/T$ but rather between $\log \rho$ and $T^{-1/4}$.

The temperature dependence of Seebeck coefficient S for the system $Nd_{2-x}Sr_xNiO_4$ was shown in Fig. 11. The samples with composition of $x \leq 0.4$ show large positive values of S below room temperature; the temperature where the sign of the S–T curve

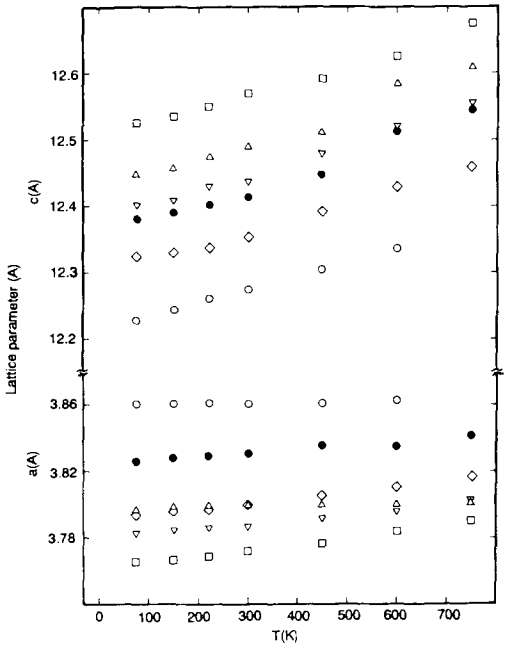

FIG. 6. Temperature dependence of cell parameters in the $Nd_{2-x}Sr_xNiO_4$ system. (●) $x = 0.0$(*Fmmm*), (○) $x = 0.0$(*Bmab*), (△) $X = 0.3$, (□) $x = 0.6$, (▽) $x = 0.9$, (◇) $x = 1.2$.

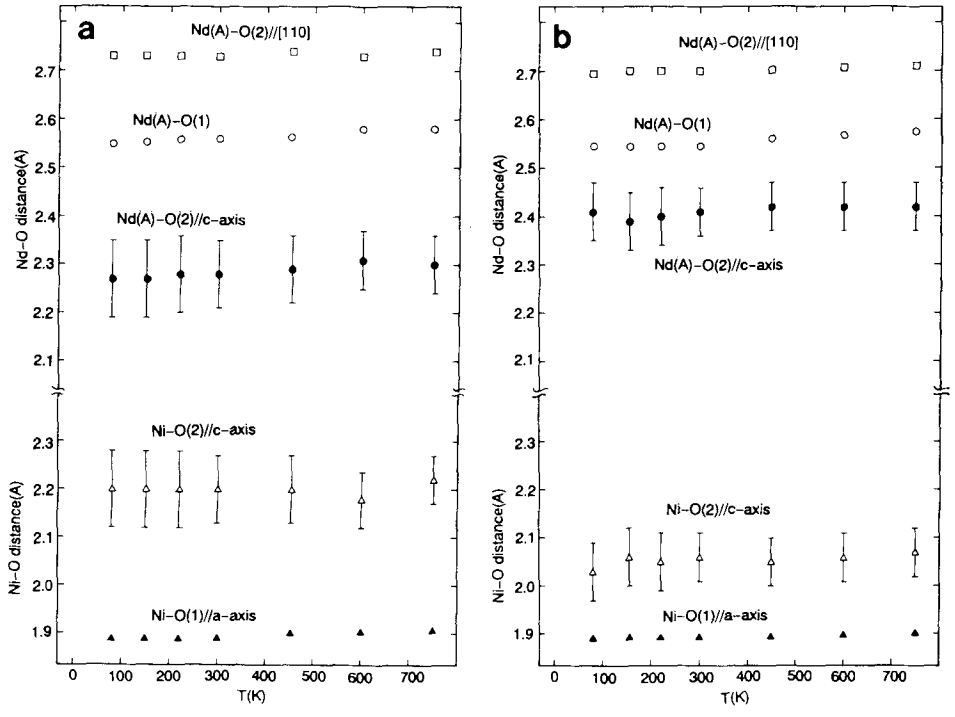

FIG. 7. Temperature dependence of bond distances in the $Nd_{2-x}Sr_xNiO_4$ system. (a) $x = 0.3$, (b) $x = 0.9$.

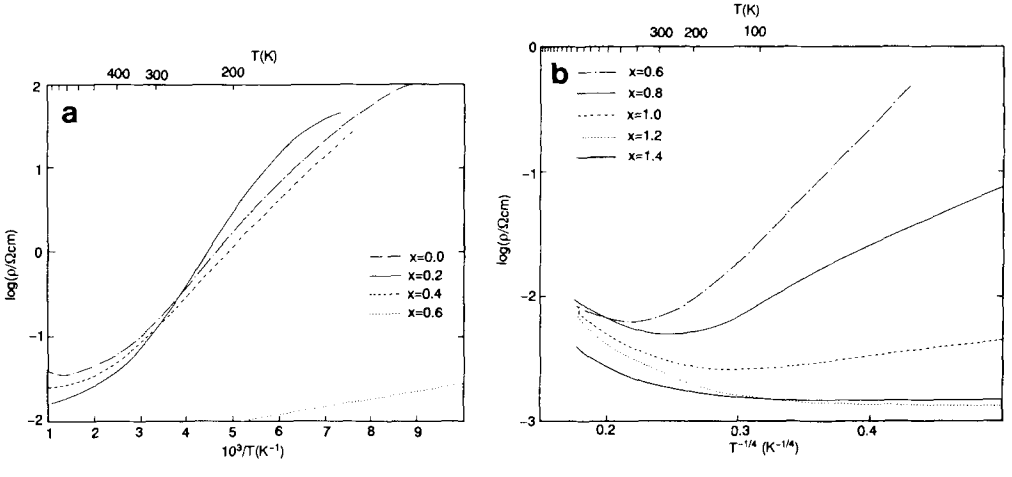

FIG. 8. Temperature dependence of electrical resistivity for $Nd_{2-x}Sr_xNiO_4$. (a) Log ρ vs. T^{-1} for $x = 0.0$–0.6, (b) Log ρ vs. $T^{-1/4}$.

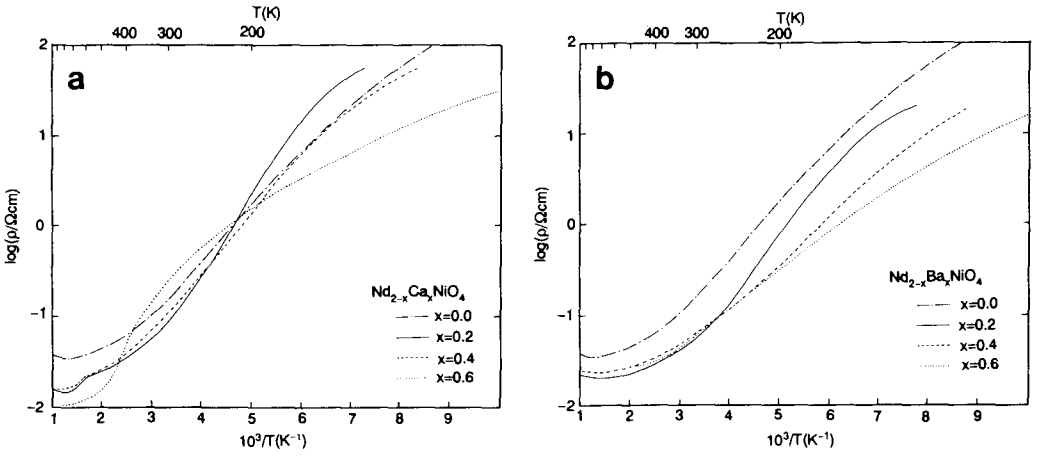

FIG. 9. Temperature dependence of electrical resistivity for $Nd_{2-x}A_xNiO_4$ (A = Ca or Ba). (a) Log ρ vs. T^{-1} for $Nd_{2-x}Ca_xNiO_4$ ($0 \leq x \leq 0.6$); (b) Log ρ vs. T^{-1} for $Nd_{2-x}Ba_xNiO_4$ ($0 \leq x \leq 0.6$).

changes from minus to plus decreases with increasing x. The dominant carrier in this region is holes but low concentration at low temperature. In the samples of $x = 0.6$ and 0.8, the sign becomes minus in all temperature ranges measured implying that the dominant carrier is electrons, while it becomes plus again at low temperatures for $x \geq 1.0$. In $x = 1.4$, it is again minus in a whole temperature range. In large Sr content regions such as $x > 1.0$, the conduction is carried out not only by the electrons but also by the holes.

The first point to be noted in the above results is the remarkable change in electrical properties at near the composition of $x \cong 0.6$ for $Nd_{2-x}A_xNiO_4$. There may be a significant change of the electronic state of the system near $x = 0.6$. This is also reflected in the variation of interatomic distances. The Ni–O(2)/Ni–O(1) axial ratio decreases monotonically with increasing x; however, the relative position of the O(2) atom shifts away from its Nd(Sr) nearest neighbor toward its Ni nearest neighbor in the compositional range $0 \leq x \leq 0.4$ where the resistivity remains high with positive carriers; this shift stops for $x \geq 0.6$ where the room tempera-

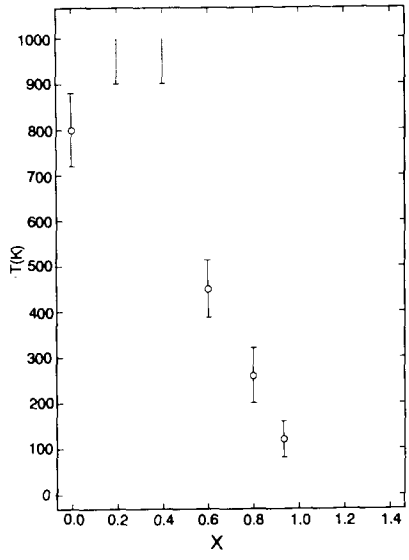

FIG. 10. Variation of the metal–semiconductor transition temperature T_t as a function of x in the $Nd_{2-x}Sr_xNiO_4$. Solid bar and open circle show the flat range and the midpoint in resistivity at the transition, respectively.

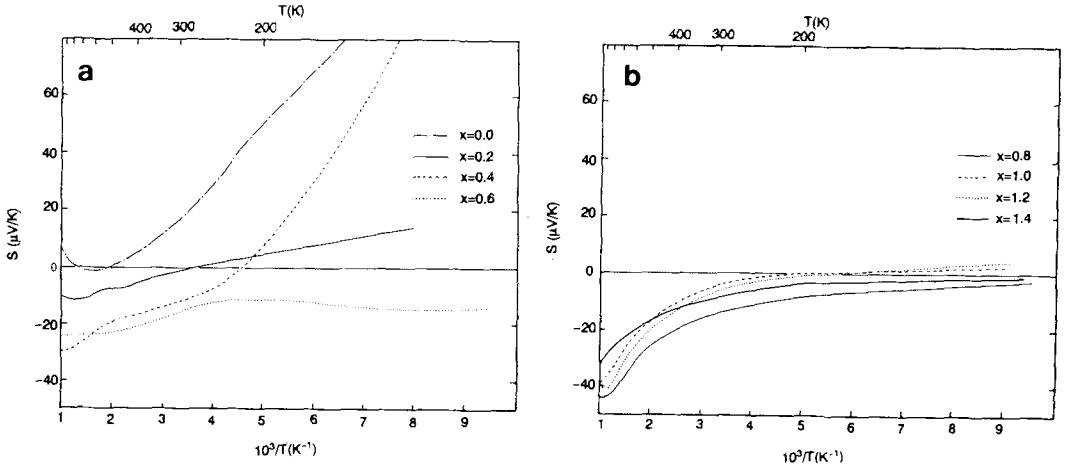

FIG. 11. Temperature dependence of the Seebeck coefficient of $Nd_{2-x}Sr_xNiO_4$. (a) $x = 0$–0.6; (b) $x = 0.8$–1.4.

ture conduction is metallic with negative carriers. However, the relationship between the O(2) position and electrical properties was not clear in the high and low temperature XRD experiment. The error bars were too large to judge the slight change in Ni–O(2) and Nd–O(2) distances. Analysis by neutron diffraction will be needed.

The electrical properties for compositions below $x \cong 0.5$ can be explained based on the mechanism for La_2NiO_4 in terms of correlation-split $\sigma^*_{x^2-y^2}$ band and a localized d_{z^2} state presented by Goodenough and Ramasesha (*17*). The $d^1_{z^2}$ energy has reasonably been considered, from the elongation of the NiO octahedron, to be lower than the mean energy of the occupied state of the half-filled $\sigma^*_{x^2-y^2}$ band. Substitution of Sr for Nd reduces the electron density in these state, forming the hole in the conduction band. However, the resistivity of $Nd_{2-x}Sr_xNiO_4$ for $x < 0.4$ remains polaronic obeying a small polaron mechanism. Above $x \cong 0.6$, the energy density state as above no longer holds. As the Ni–O(2) bond distance along the c axis approaches the basal Ni–O(1) distance, causing an upward shift of the $d^1_{z^2}$ level, it is possible that the residual electrons tend to populate the $\sigma^*_{x^2-y^2}$ band more preferentially than the d_{z^2} level. The decrease in the electron density and the manner of population would effectively reduce the correlation splitting of the $\sigma_{x^2-y^2}$ band. The tendency toward metal which becomes almost perfect at $x = 1.0$ can thus be qualitatively explained. Another point to be considered is a probable change in the cationic and anionic components of the $\sigma_{x^2-y^2}$ band. The basal Ni–O(1) distance remains almost constant, but the change in the formal charge of nickel from $+2$ ($x = 0$) to $+3$ ($x = 1$) and further to $+4$ ($x = 2$) is expected to lower the $3d\gamma$ levels with respect to the O_{2p} levels, thus enhancing the contribution of the latter to the $\sigma_{x^2-y^2}$ band.

Conclusion

In summary, we have synthesized a solid solution of $Nd_{2-x}A_xNiO_4$ (A = Ca; $0 \le x \le 0.6$, Sr; $0 \le x \le 1.4$, and Ba; $0 \le x \le 0.6$) and studied their structural and electrical properties. A Reitveld analysis of the room temperature powder XRD data showed that the tetragonal distortion of the NiO_6 octahedra decreased monotonically with increas-

ing x for $0 \leq x \leq 1.4$ in the Sr system, but the Nd(Sr)–O(2) bond length increased anomalously in the interval $0 \leq x \leq 0.6$. A semiconductor–metal transition decreased with increasing x, but it exhibited a change in character at $x = 0.6$. The measurement of the Seebeck coefficient also showed the existence of a change in conduction mechanism at $x = 0.6$.

Acknowledgments

This study was financially supported by a Grant-in-Aid for Scientific Research on Chemistry of New Superconductors from the Ministry of Education, Science, and Culture. All computations for structural analysis were carried out at the Mie University Information Processing Center.

References

1. J. G. Bednortz and K. A. Muller, *Z. Phys. B* **61,** 189 (1986).
2. J. B. Goodenough and J. M. Longo, *Landolt-Bornstein Tabellen* **III/49,** 193 (1970).
3. P. Ganguly and C. N. Rao, *Mater. Res. Bull.* **8,** 405 (1973).
4. C. N. Rao, D. J. Buttrey, N. Otsuka, P. Ganguly, H. R. Harrison, C. J. Sandberg, and J. H. Honig, *J. Solid State Chem.* **67,** 266 (1984).
5. M. Sayer and P. Odier, *J. Solid State Chem.* **67,** 26 (1987).
6. Z. Hiroi, T. Obata, M. Takano, Y. Bando, Y. Takeda, and O. Yamamoto, *Phys. Rev. B* **41,** 11665 (1990).
7. J. Gopalakrishnan, G. Colsman, and B. Beuter, *J. Solid State Chem.* **22,** 145 (1977).
8. Y. Takeda, R. Kanno, M. Sakano, O. Yamamoto, M. Takano, Y. Banndo, H. Akinaga, K. Takita, and J. B. Goodenough, *Mater. Res. Bull.* **25,** 293 (1990).
9. D. J. Buttrey and J. M. Honig, *J. Solid State Chem.* **72,** 38 (1988).
10. B. W. Arbuckle, K. V. Ramanujachary, Zhen Zhang, and M. Greenblatt, *J. Solid State Chem.* **88,** 278 (1990).
11. F. Izumi, *J. Mineral Soc. Jpn.***17,** 37 (1985).
12. R. D. Shannon, *Acta Crysallogr. Sect. A: Found. Crystallogr.* **32,** 751 (1976).
13. J. B. Goodenough and A. Manthiram, *J. Solid State Chem.* **88,** 115 (1990).
14. A. B. Austin, L. G. Garreiro, and J. V. Marzik, *Mater. Res. Bull.* **24,** 639 (1989).
15. J. D. Jorgensen, B. Dabrowski, Shiyou Pei, D. R. Richards, and D. G. Hinks, *Phys. Rev. B* **40,** 2189 (1989).
16. B. Grande and H. Muller-Buscham, *Z. Anorg. Allg. Chem.* **433,** 152 (1977).
17. J. B. Goodenough and S. Ramasesha, *Mater. Res. Bull.* **17,** 383 (1982).